Geometrically Nonlinear Transient Deflection Behaviour of a Functionally Graded Porous Skew Plate Subjected to Thermal Loads

Naveen Kumar H S [1, *]

[1] *Department of Mechanical Engineering, Government Polytechnic, Hiriyur, Karnataka-577599, India.*

Abstract: *This research paper delves into the impact of porosity distributions with geometrical skewness of a functionally graded porous skew (FGPS) plate on the geometrically nonlinear transient deflections in a thermal environment. A modified power-law series characterised the temperature-dependent effective material properties in the thickness direction. The nonlinear finite element model of the plate was made using the first-order shear deformation (FSD) theory, and the governing equations were found using von Kármán's assumptions and Hamilton's principle. To solve the nonlinear equations, Newmark's integration approach was utilised. The study looked at the geometrically nonlinear transient responses of the FGPS plate under thermal loads for different geometrical skewness and system parameters. The results indicate that both the porosity distribution and temperature fields significantly influence the geometrically nonlinear transient deflections of the FGPS with geometric non-uniformities.*

Keywords: **Functionally graded porous plates; Geometric non-uniformities; Temperature; Nonlinear transient deflections.**

1. Introduction

Functionally graded materials (FGMs) are highly advanced composite materials that have attracted researchers and engineers recently due to their outstanding performance. The FGMs exhibit continuous and controlled changes in their properties in a predetermined direction based on temperature. It is typically composed of two materials, namely ceramic and metal. As an outcome, FGMs can mitigate the primary issues of composite materials, such as interfaces, thermal stresses, stress concentration, residual stresses, fractures, and delamination. However, during the production of FG plates, it is difficult to avoid the occurrence of porosities due to the limitations of the fabrication technique. Inserting the first and second constituent materials into the middle section of the functionally graded (FG) plate without creating porosities is also challenging. Moreover, porosities can arise due to the varying solidification temperatures of the two materials [1]. These porosities can weaken the strength of FGMs. Therefore, it is crucial to investigate the effect of porosities when analysing FGM plates.

In addition, when designing FG rectangular plates, integrating skewness into the geometry of the plate provides multiple alignment options for obstacles. This skewing also reduces the plate's surface area, thereby increasing its rigidity. As a consequence, FGMs are the optimal option for a variety of structural applications in high-temperature environments, especially for skew plates, due to their enhanced mechanical properties. The existing body of research primarily concentrates on the investigation of nonlinear vibration studies and dynamic responses of FGMs structures with porosity [2–5], with a particular emphasis on beams and rectangular plates [6,7]. Despite the potential benefits of functionally graded skew (FGS) plates for engineers in aligning plate edges during complex situations, these components have not received significant attention. The variation in the area of the plate is directly proportional to its skewness, which in turn has a proportional effect on its stiffness.

The nonlinear behaviour of the plate is significantly affected by skewness. Skew plates find applications in diverse industries such as aerospace, civil, mechanical, biomedical, and defence [8]. Much of the research works are provided for the less skewed FG plates without considering the porosities. The investigation focuses on the static and dynamic analysis, free and forced vibrations of the skewed FG plates subjected to with and without thermal loads in the finite element (FE) framework, and analytical methods with various shear deformation theories in conjunction with von Kármán nonlinearities [9–13].

Based on a comprehensive analysis of existing literature, it has been observed that there is a lack of studies investigating the impact of porosities and temperature on the geometrically nonlinear transient deflection of geometrically skewed FG porous plates. This article aims to examine the effect of porosity distributions on the thermal behaviour of FG plates with geometrical skewness. The solutions are obtained by utilising Newmark's integration method for the model that has been developed using nonlinear FE procedures based on the first-order shear deformation (FSD) theory and von Kármán assumptions in a thermal environment. The study thoroughly investigates the significant impact of porosity distributions and geometrical skewness on the geometrically nonlinear transient deflections of the FGPS plate under various thermal loadings. The investigation considers different system parameters to provide a comprehensive analysis.

2. Materials and Method

The length a, width b, and thickness t are the dimensional parameters of the FGPS plate depicted in Figure 1. The skew of the plate is taken into account by rotating the y-axis at an angle termed the skew angle (Φ). The FGPS plate is composed of two isotropic constituent materials: ceramic and metal. The top of the FGPS plate $(z = t/2)$ is made of ceramic, and the bottom surface $(z = -t/2)$ is made of metal only. The volume fraction of ceramic material (V_c) differs unceasingly through the thickness direction in the plate, i.e., the z-axis, as shown in Figure 1.

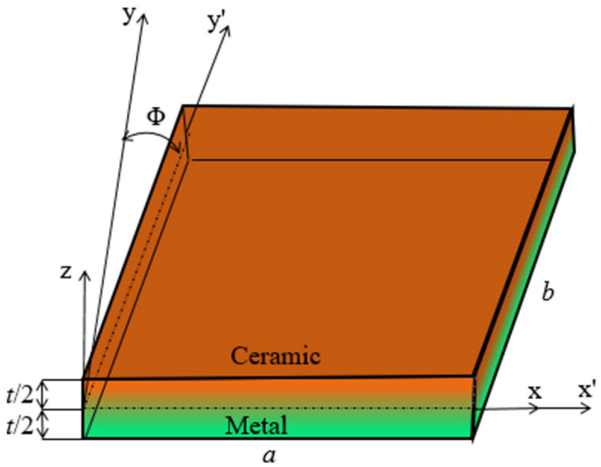

Figure 1. The FGPS plate's geometry.

The generalised temperature and position-dependent effective material properties (EMP) of the FGPS plate can be written in the framework of the modified power-law series [14] as.

$$\mathrm{P}_{\mathrm{fg}}\left(\mathrm{Z},\mathrm{T}\right) = \left(P_t(\mathrm{T}) - P_b(\mathrm{T})\right)V_c + P_b(\mathrm{T}) - \left(\frac{e_p}{2}\right)\left[P_t(\mathrm{T}) + P_b(\mathrm{T})\right]P_d \tag{1}$$

where e_p ($e_p << 1$) is the porosity volume index (PVI). The PVI determines the volume of porosities present in the FGS plate. For an ideal (porosity-free) FGS plate, the PVI (e_p) is

zero. $P_b(T)$ and $P_t(T)$ are the temperature-dependent material properties, and P_d refers to a generic representation of different types of distributions of porosity. The following are the various distributions of porosities in the FGPS plate that are considered for the study in a thermal environment.

(1) *Evenly dispersed porosities (EDP) (P_e)*: The porosities are dispersed uniformly across the FGPS plate thickness, as depicted in Figure 2 (a). Besides, the temperature-dependent EMP of the plate with EDP can be expressed by placing the value $P_d = 1$ in Eq. 1, and the modified equation is:

$$\mathrm{P_{fg}}\left(\mathrm{Z,T}\right) = \left(P_t\left(\mathrm{T}\right) - P_b\left(\mathrm{T}\right)\right)V_c + P_b\left(\mathrm{T}\right) - \left(\frac{e_p}{2}\right)\left[P_t\left(\mathrm{T}\right) + P_b\left(\mathrm{T}\right)\right] \tag{2}$$

(2) *Centrally dispersed porosity (CDP) (P_c)*: The middle section of the FGPS plate has the most significant porosity density, as depicted in Figure 2 (b). Also, the temperature-dependent EMP of the plate with CDP can be written as follows:

replacing $P_d = \left(1 - \frac{2|\mathrm{Z}|}{t}\right)$ in Eq. 1, we obtain,

$$\mathrm{P_{fg}}\left(\mathrm{Z,T}\right) = \left(P_t\left(\mathrm{T}\right) - P_b\left(\mathrm{T}\right)\right)V_c + P_b\left(\mathrm{T}\right) - \left(\frac{e_p}{2}\right)\left[P_t\left(\mathrm{T}\right) + P_b\left(\mathrm{T}\right)\right]\left(1 - \frac{2|\mathrm{Z}|}{t}\right) \tag{3}$$

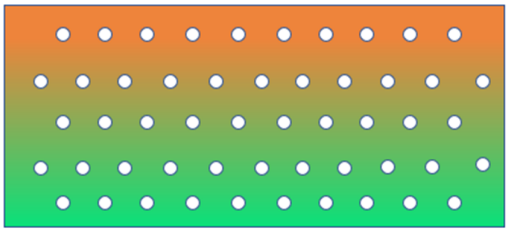

(a)

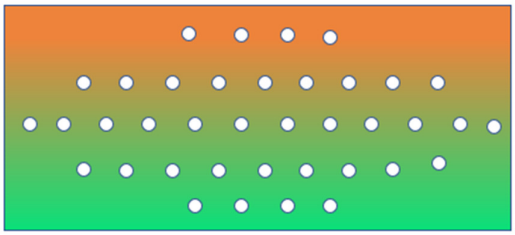

(b)

Figure 2. Distribution of porosities in FGPS plate (a) EDP (P_e), and (b) CDP (P_c).

The temperature distribution is presumed to occur in the path of gradation. A steady-state one-dimensional Fourier heat conduction equation can be used to solve temperature distribution. A thermal field is assumed to be constant in any *x-y* plane of the FGPS plate. The temperature distribution through the thickness can thus be solved using the steady-state heat transfer equation as follows [15,16] :

$$-\frac{\mathrm{d}}{\mathrm{dx}}\left[k(z)\frac{\mathrm{dT}}{\mathrm{d}z}\right] = 0 \tag{4}$$

3. Kinematics of Deformations

The plate model in the current analysis is developed using the FSD theory [17] in conjunction with von Karman stain-displacement geometric nonlinearity. The relationships for strain-displacements can be expressed as follows [18]

$$\{\varepsilon_b\}=\{\varepsilon_{xx}\ \varepsilon_{yy}\ \gamma_{xy}\}^T;\ \{\varepsilon_s\}=\{\gamma_{xz}\ \gamma_{yz}\}^T \tag{5}$$

$$\varepsilon_{xx}=\frac{\partial u_1}{\partial x}+Z\frac{\partial \theta_x}{\partial x}+\frac{1}{2}\left(\frac{\partial w_1}{\partial x}\right)^2;\ \varepsilon_{yy}=\frac{\partial v_1}{\partial y}+Z\frac{\partial \theta_y}{\partial y}+\frac{1}{2}\left(\frac{\partial w_1}{\partial y}\right)^2$$

$$\gamma_{xy}=\frac{\partial u_1}{\partial y}+\frac{\partial v_1}{\partial x}+Z\left(\frac{\partial \theta_x}{\partial y}+\frac{\partial \theta_y}{\partial x}\right)+\frac{\partial w_1}{\partial x}\frac{\partial w_1}{\partial y};$$

$$\gamma_{xz}=\theta_x+\frac{\partial w_1}{\partial x};\ \gamma_{yz}=\theta_y+\frac{\partial w_1}{\partial y} \tag{6}$$

where u_1, v_1, and w_1 are the generic displacements in the direction of x, y, and z- coordinates, respectively, at a reference point (x, y) lying on the FGPS plate's midplane (Z = 0). The corresponding generic rotations of a normal to the point of reference at a reference plane along the y- and x-axis, respectively, are θ_x, and θ_y. The strain vectors $\{\varepsilon_b\}$ and $\{\varepsilon_s\}$ can express the state of strain for any specified point in the whole FGPS plate. However, $\{\varepsilon_b\}$ comprises in-plane normal strain and transverse normal strain and $\{\varepsilon_s\}$ comprises the shear strain in the transverse direction.

At any position on the plate, the in-plane and transverse shear strain vectors can indeed be described as follows [19,20]:

$$\{\varepsilon_b\}=\{\varepsilon_{tb}\}+z\{\varepsilon_{rb}\}+\{\varepsilon_{tbNL}\};\ \{\varepsilon_s\}=\{\varepsilon_{ts}\}+\{\varepsilon_{rs}\} \tag{7}$$

where the general strain vectors $\{\varepsilon_{tb}\}$, $\{\varepsilon_{rb}\}$, $\{\varepsilon_{tbNL}\}$, $\{\varepsilon_{ts}\}$ and $\{\varepsilon_{rs}\}$ arises in Eq. 7 can be written as follows:

$$\{\varepsilon_{tb}\}=\left[\frac{\partial u_1}{\partial x}\ \frac{\partial v_1}{\partial y}\ \frac{\partial u_1}{\partial y}+\frac{\partial v_1}{\partial x}\right]^{\mathrm{T}};$$

$$\{\varepsilon_{tbNL}\}=\left[\frac{1}{2}\left(\frac{\partial w_1}{\partial x}\right)^2\ \frac{1}{2}\left(\frac{\partial w_1}{\partial y}\right)^2\ \frac{\partial w_1}{\partial x}\frac{\partial w_1}{\partial y}\right]^{\mathrm{T}}$$

$$\{\varepsilon_{rb}\}=\left[\frac{\partial \theta_x}{\partial x}\ \frac{\partial \theta_y}{\partial y}\ \frac{\partial \theta_x}{\partial y}+\frac{\partial \theta_y}{\partial x}\right]^{\mathrm{T}};\ \{\varepsilon_{ts}\}=\left[\frac{\partial w_1}{\partial x}\ \frac{\partial w_1}{\partial y}\right]^T;\ \{\varepsilon_{rs}\}=\left[\theta_x\ \theta_y\right]^{\mathrm{T}} \tag{8}$$

For any position in the entire FGPS plate, the state of stress and associated state of strain are defined as follows [9]:

$$\{\sigma_b\}=\left[Q_b(Z,\mathrm{T})\right]\left(\{\varepsilon_b\}-\{\alpha\}\Delta\mathrm{T}\right);\ \{\sigma_s\}=\left[Q_s(Z,\mathrm{T})\right]\{\varepsilon_s\} \tag{9}$$

where $\{\sigma_b\}=\{\sigma_{xx}\ \sigma_{yy}\ \tau_{xy}\}^{\mathrm{T}}$ and $\{\sigma_s\}=\{\tau_{xz}\ \tau_{yz}\}^{\mathrm{T}}$

$$\{\alpha\}=\left[\alpha_x(Z,\mathrm{T})\ \alpha_y(Z,\mathrm{T})\ 0\right]^{\mathrm{T}} \quad \text{and} \quad \Delta\mathrm{T}=\mathrm{T}(Z)-\mathrm{T}_0 \tag{10}$$

The normal stresses σ_{xx} and σ_{yy} are in the x- and y- directions, respectively, are represented by the terms in Eq. 10. In-plane and transverse shear stresses are given by τ_{xy}, τ_{xz}, and τ_{yz} respectively. $\left[Q_b(\mathrm{Z},\mathrm{T})\right]$ and $\left[Q_s(\mathrm{Z},\mathrm{T})\right]$ are the elastic coefficient matrices and the function of the Z- coordinate. $\alpha_x(\mathrm{Z},\mathrm{T})$ and $\alpha_y(\mathrm{Z},\mathrm{T})$ are the coefficients of thermal expansion in x- and y- directions, respectively; T(*Z*) is the temperature for any point in the FGPS plate, T_0 is the reference temperature, and ΔT is the rise in temperature over the reference temperature.

$$\left[Q_b(Z,\mathrm{T})\right]=\begin{bmatrix} Q_{11} & Q_{12} & 0 \\ Q_{12} & Q_{22} & 0 \\ 0 & 0 & Q_{66} \end{bmatrix};\ \left[Q_s(Z,\mathrm{T})\right]=k_s\begin{bmatrix} Q_{55} & 0 \\ 0 & Q_{44} \end{bmatrix} \tag{11}$$

in Eq. 11, $k_s=\pi^2/12$ can be termed as shear correction coefficient.
From Eq. 11, the expressions for elastic coefficients can be stated as follows:

$$Q_{11}=Q_{22}=\frac{E_{fg}(\mathrm{Z},\mathrm{T})}{1-\left(\vartheta_{fg}(\mathrm{Z})\right)^2} \quad Q_{12}=Q_{21}=\frac{\vartheta_{fg}(\mathrm{Z})E_{fg}(\mathrm{Z},\mathrm{T})}{1-\left(\vartheta_{fg}(\mathrm{Z})\right)^2};$$

$$Q_{44}=Q_{55}=Q_{66}=\frac{E_{fg}(\mathrm{Z},\mathrm{T})}{2\left(1+\vartheta_{fg}(\mathrm{Z})\right)} \tag{12}$$

where $E_{fg}(\mathrm{Z},\mathrm{T})$ and $\vartheta_{fg}(\mathrm{Z})$ are the effectual Young's modulus and effectual Poisson's ratio of the FGPS plate, respectively.
The total potential energy of the entire FGPS plate in terms of the first variation can be expressed as follows by engaging Hamilton's principle [21]:

$$\delta T_p=\int_0^a\int_0^b\left[\frac{1}{2}\int_{-t/2}^{t/2}\left(\delta\{\varepsilon_b\}^T\{\sigma_b\}+\delta\{\varepsilon_s\}^T\{\sigma_s\}+\delta\{d_t\}^T\ \rho\left\{\ddot{d}_t\right\}\right)dz-\delta\{d_t\}^T\{F\}\right]dx\,dy$$

(13)

where $\{\mathrm{F}\}=\{0\ 0\ \mathrm{p}\}^{\mathrm{T}}$ is externally applied force acting on the plate's surface, *p* is the load in the transverse direction, and the first variation is defined as δ.

4. Nonlinear Finite Element Modelling

The complete FGPS plate is divided into several iso-parametric elements. Each element has eight nodes; meanwhile, each node comprises three translational and two rotational degrees of freedom[18]. The general displacement vectors $\{d_{tn}\}$ and $\{d_{rn}\}$ linked with the node n (n = 1,2,3, …,8) of an element are expressed as follows [22]:

$$\{d_{tn}\}=\left[u_{1n}\ v_{1n}\ w_{1n}\right]^{\mathrm{T}} \text{ and } \{d_{rn}\}=\left[\theta_{xn}\ \theta_{yn}\right]^{\mathrm{T}} \tag{14}$$

Further, for any specified point in an element, the general displacement vectors can be stated as

$$\{d_t\}=\left([N_t]\{d_t^e\}\right) \text{ and } \{d_r\}=\left([N_r]\{d_r^e\}\right) \tag{15}$$

in which, $\{d_t^e\}$ and $\{d_r^e\}$ are the displacement vectors of the nodal translational and nodal rotational degrees of freedom, respectively; $[N_t]$ and $[N_r]$ represent the matrices in the order (3×24) and (2×16) of the shape function, respectively.

The generic strain vectors for any point within an element are extracted as follows from Eqs.7 and 15.

$$\{\varepsilon_{tb}\}=[ß_{tb}]\{d_t^e\}\ ;\ \{\varepsilon_{tbNL}\}=\frac{1}{2}[ß_1][ß_2]\{d_t^e\};\ \{\varepsilon_{rb}\}=[ß_{rb}]\{d_r^e\}$$

$$\{\varepsilon_{ts}\}=[ß_{ts}]\{d_t^e\} \text{ and } \{\varepsilon_{rs}\}=[ß_{rs}]\{d_r^e\} \tag{16}$$

in which, $[ß_{tb}]$, $[ß_1]$, $[ß_2]$, $[ß_{rb}]$, $[ß_{ts}]$ and $[ß_{rs}]$ are the generalised nodal strain displacement matrices.

Deputizing Eqs. 7, 9, and 16 in Eq. 13 and employing the principle of total potential energy, i.e., $\delta T_p^{\ e}=0$, and condensing; the elemental equations of motion can be obtained as follows[13]:

$$\left[\left(\mathrm{M}^{\mathrm{e}}\right)\right]\left\{\ddot{d}_t^{\ e}\right\}+\left[K_{tt}^{\ e}\right]\left\{d_t^{\ e}\right\}+\left[K_{tr}^{\ e}\right]\left\{d_r^{\ e}\right\}=\left\{\mathrm{F}_t^{\ e}\right\} \tag{17}$$

$$\left[K_{rt}^{\ e}\right]\left\{d_t^{\ e}\right\}+\left[K_{rr}^{\ e}\right]\left\{d_t^{\ e}\right\}=0 \tag{18}$$

in which, $\left[\left(\mathrm{M}^{\mathrm{e}}\right)\right]$ is termed as the elemental mass matrix of an element, $\left[K_{tt}^e\right]$, $\left[K_{tr}^e\right]$, $\left[K_{rt}^e\right]$ and $\left[K_{rr}^{\ e}\right]$ can be described as the elastic stiffness matrices of an element and $\left\{\mathrm{F}_t^e\right\}$ is the load vector of an element. The global equations of equilibrium are obtained by assembling the elemental governing equations into the global space. The global rotational degrees of freedom are condensed to extract the global equilibrium equations relating to the global nodal translational degrees of freedom after imposing the boundary conditions.

$$[\mathrm{M}]\left\{\ddot{X}_t\right\}+\left[\left(K_{eq}\right)-\left(K_G\right)\right]\{(\mathrm{X}_t)\}=\{\mathrm{F}\} \tag{19}$$

where,

$$\left[\left(K_{eq}\right)\right]=\left[\left(K_{tt}\right)\right]-\left(\left[\left(K_{tr}\right)\right]\left[\left(K_{rr}\right)\right]^{-1}\left[\left(K_{rt}\right)\right]\right) \tag{20}$$

$[K_G]$ is the geometric stiffness matrix, and the plate experiences geometric distortion due to thermal load that occurs through the nonlinear temperature distribution via the thickness of the FGPS plate. This induces thermal stresses and has a direct impact on the FGPS plate's deflection characteristics. As a result of the deformed geometry of the FGPS plate generated by thermal forces, it necessitates the measurement of the geometric stiffness matrix [23].

$$K_G=K_{Gb}+K_{Gs} \tag{21}$$

Further, the eigenvalues and corresponding eigenvectors of the FGPS plate can be obtained by rearranging Eq. 19 as follows:

$$\left(\left[\left(K_{eq}-K_G\right)\right]-\left(\omega^2\left[\mathrm{M}\right]\right)\right)\{\mathrm{X}\}=0 \tag{22}$$

where ω and X are the FGPS plate's natural frequency and corresponding eigenvector, respectively.

5. Skew Boundary Transformation

In order to impose boundary conditions on the skew edges of the FGPS plate, it is essential to transform the Cartesian coordinate's axes along the x' -, y'- directions, as shown in Figure 1. Therefore, the generalised displacement vectors of a point resting on the skew edge are transformed as follows [24]:

$$\{d_t\}=[T_t]\{d_t^1\}\ ;\ \{d_r\}=[T_r]\{d_r^1\} \tag{23}$$

where the transformed translational displacement $\{d_t^1\}$ and rotational displacement $\{d_r^1\}$ components are expressed as follows:

$$\{d_t^1\}=\left[u_1^1\ v_1^1\ w_1^1\right]^{\mathrm{T}};\ \{d_r^1\}=\left[\theta_x^1\ \theta_y^1\right]^{\mathrm{T}} \tag{24}$$

For a given node, the transformation matrices that act on the translational $[T_t]$ and rotational $[T_r]$ degrees of freedom along the main diagonals can be written as follows:

$$[T_t]=\begin{bmatrix}\cos\phi & \sin\phi & 0\\ -\sin\phi & -\cos\phi & 0\\ 0 & 0 & 1\end{bmatrix};\ [T_r]=\begin{bmatrix}\cos\phi & \sin\phi\\ -\sin\phi & \cos\phi\end{bmatrix} \tag{25}$$

As a result, from these transformations, the transformed stiffness and mass matrices yield as follows:

$$\left[\bar{K}_{tt}^e\right]=\left[T_t\right]^T\left[K_{tt}^e\right]\left[T_t\right];\ \left[\bar{K}_{tr}^e\right]=\left[T_t\right]^T\left[K_{tr}^e\right]\left[T_r\right];$$

$$\left[\bar{K}_{rr}^e\right]=\left[T_r\right]^T\left[K_{rr}^e\right]\left[T_r\right];\ \left[\bar{M}^e\right]=\left[T_t\right]^T\left[M^e\right]\left[T_t\right] \tag{26}$$

The geometrically nonlinear transient deflections are determined by utilising Newmark's integration method [9,25]. The detailed procedure for Newmark's integration method to extract the geometrically nonlinear transient deflections, is presented in Naveen et al. [13].

6. Results And Discussions

The FGPS plate is considered to investigate the effects of porosities and geometrical skewness on the geometrically nonlinear transient deflections subjected to thermal loads. A ceramic surface on top of the plate and a metallic surface on the plate's bottom compose the FGPS plate. At the same time, these two constituent materials are graded, incorporating the porosity distributions. Various validation studies have been carried out to check the accuracy of the proposed nonlinear FE model. Table 1 provides the temperature-dependent properties of the materials Si_3N_4 and SUS304 used in the present investigation. Multiple parameters are considered in parametric studies to investigate the geometrically nonlinear transient responses of the FGPS plate.

Table 1. Coefficients of the temperature-dependent constituent materials Si_3N_4 and SUS304: Young's modulus E (Pa) and the coefficient of thermal expansion α (1/K) [26].

Materials	Properties	ς_0	ς_{-1}	ς_1	ς_2	ς_3	P (T = 300 K)
Si_3N_4	E (Pa)	348.43e9	0.0	-3.070e-4	2.160e-7	-8.946e-11	322.2715e9
	α (1/K)	5.8723e-6	0.0	9.095e-4	0.0	0.0	7.4746e-6
SUS304	E (Pa)	201.04e9	0.0	3.079e-4	-6.534e-7	0.0	207.7877e9
	α (1/K)	12.330e-6	0.0	8.086e-4	0.0	0.0	15.321e-6

6.1. Validation

The dimensionless fundamental frequency for a simply supported Si_3N_4 / SUS304 FG square plate under thermal loading is compared with Huang and Shen's [14] results for different volume fraction grading index (VFGI), *m*. The plate's ceramic surface is exposed to two different thermal loadings (T_c), 400 K and 600 K, respectively. The metal surface has a temperature (T_m) of 300 K. Figure 3 shows that the current model's results are very similar to those reported in the reference literature [14]. Besides, [8 × 8] mesh size is considered sufficient to model the FGPS plate based on progressive mesh refinement. Further, the fundamental natural frequency is computed to check the reliability of the present model on the skewness of the isotropic plate with skew angles of 0°, 15°, 30°, and 45°. Table 2 shows that the findings presented in the table agree very well with the reference literature [27]. To further validate the porosity results, the dimensionless frequency for FG plate with porosity is evaluated and compared to Rezaei et al. [28]. Table 3 shows that the findings on both EDP (P_e) and CDP (P_c) distributions are in solid agreement with the reference [28].

Table 2. The dimensionless natural frequency comparison for an isotropic skew plate (*a/b* = 1, SSSS).

a/t	Ref.	Skew angle (Φ)			
		0°	15°	30°	45°
10	Present	1.9491	2.0945	2.5447	3.4285
	Ref. [27]	1.9311	2.0379	2.4195	3.3548
5	Present	1.8170	1.9084	2.2035	2.7864
	Ref. [27]	1.7661	1.8560	2.1719	2.9129

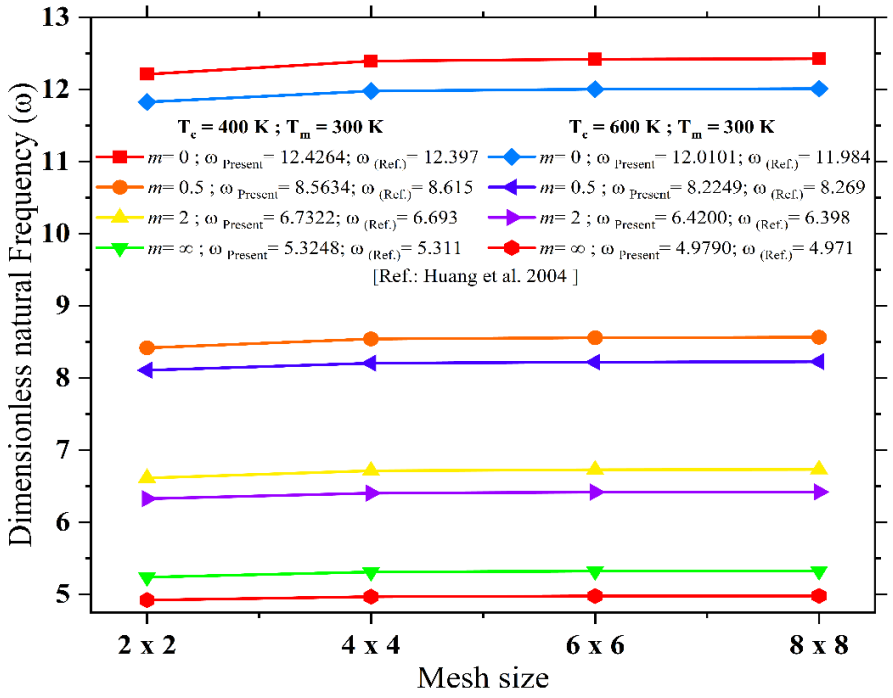

Figure 3. Comparison of fundamental natural frequency for simply supported Si_3N_4 / SUS304 square FG plate under thermal loading. (*a* = *b* = 0.2, *a*/*t* = 8).

Table 3. Dimensionless natural frequency comparison for various VFGI of FG porous plate (*a*/*b*=1, *a*/*t*=10, and SSSS).

b/*a*	e_p	Ref. [28]	$\alpha = 0$		$\alpha = 0.5$		$\alpha = 1$	
			P_e	P_c	P_e	P_c	P_e	P_c
h/*a* = 0.05								
1	0	Ref. [28]	0.0291	0.0291	0.0247	0.0247	0.0222	0.0222
		Present	0.0292	0.0292	0.0247	0.0247	0.0223	0.0223
	0.2	Ref. [28]	0.0300	0.0300	0.0246	0.0252	0.0210	0.0225
		Present	0.0296	0.0299	0.0242	0.0251	0.0207	0.0224
	0.4	Ref. [28]	0.0314	0.0310	0.0242	0.0259	0.0182	0.0227
		Present	0.0305	0.0308	0.0235	0.0257	0.0177	0.0225
h/*a* = 0.1								
0.5	0	Ref. [28]	0.0719	0.0719	0.0610	0.0610	0.0550	0.0550
		Present	0.0721	0.0721	0.0611	0.0611	0.0551	0.0551
	0.2	Ref. [28]	0.0742	0.0740	0.0607	0.0624	0.0521	0.0555
		Present	0.0732	0.0739	0.0599	0.0622	0.0513	0.0554
	0.4	Ref. [28]	0.0775	0.0765	0.0599	0.0640	0.0450	0.0561
		Present	0.0755	0.0762	0.0584	0.0636	0.0438	0.0557

Besides, the proposed model is validated with Chen et al. [29] to verify the reliability and accuracy of the methodology used for the study of geometrically nonlinear transient deflection for an orthotropic plate. Compared to reference [29], the dimensionless geometrically nonlinear transient deflection exhibits a very similar response, as shown in Figure 4.

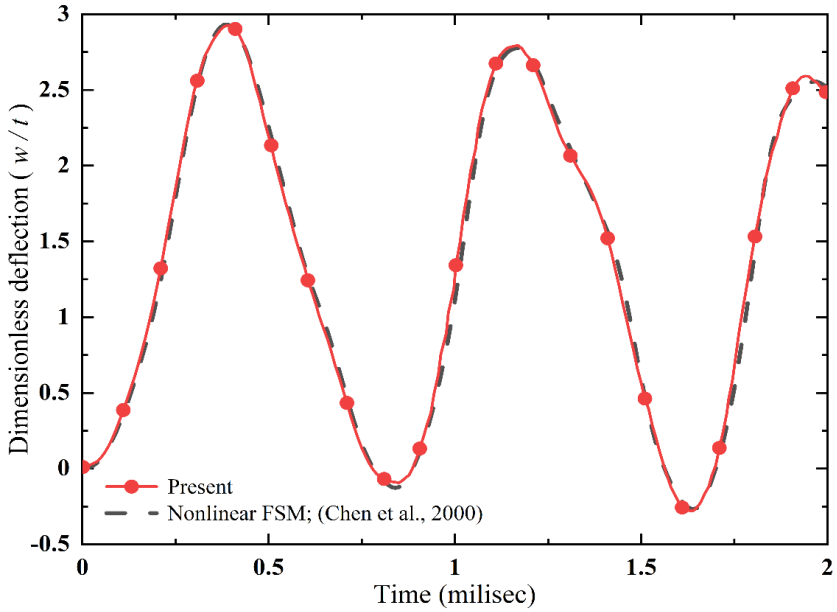

Figure 4. The dimensionless nonlinear transient deflections of the SSSS orthotropic plate.

7. Numerical results

According to the comparative studies in section 6.1, the present model gives a consistent result for the parametric studies of the FGPS plate. Besides, to obtain all parametric study data, the mesh size [8×8] considered for validation is used. The FGPS plate has a mixture of materials such as Si_3N_4 / SUS304. The FGPS plate is assumed to undergo one-dimensional heat conduction along the thickness direction. The resulting nonlinear temperature distribution is calculated using Eq (4). The reference temperature (T_0) and the temperature on the metal surface (T_m) is assumed to be 300 K. The properties such as thermal conductivity, density, and Poisson's ratio of the ceramic and metal constituents are presumed to be independent of temperature, as they are weakly dependent on temperature changes. The mass density (ρ_c) and thermal conductivity (kc) for ceramic material (silicon nitride - Si_3N_4) are 2370 kg / m^3 and 9.19 W / m K, respectively meanwhile; 8166 kg/m^3 and 12.04 W/m K are the mass density (ρm) and thermal conductivity (km) of metal (stainless steel - SUS304), respectively. The thermal expansion coefficient and Young's modulus depend on the temperature, as shown in Table 1. For Si_3N_4 / SUS304, the Poisson's ratio is presumed to be constant at 0.28. A uniform step load of q_0 = 1 N/mm^2, a time step of $\Delta t_i = 1\times10^{-5}$, and a dimensionless central deflection function $\breve{w}_c = w/t$ are used for this analysis.

7.1. Effect of Porosity volume index and skew angle

The significance of porosity distributions on the geometrically nonlinear transient deflection of the FGPS plate in a thermal environment is investigated in this section. The effects of skew angle, temperature gradient, porosity distributions, PVI, and VFGI are analysed on the geometrically nonlinear transient deflection. For EDP (P_e) and CDP (P_c) type porosity distributions, the effect of PVI (e_p) = 0.1, 0.2, and 0.3 on different skew angles (Φ) 0° and 40° is considered. Figures. 5 - 8 reveal that the amplitude and time period of motion decrease as the skew angle increases. This may be due to an increase in the stiffness of the plate as the skew angle increases. In addition, the PVI affects the deflection due to the variance in the bending stiffness and the thermal strains in the presence of porosities. Consequently, at lower temperatures (T_c = 400 K), a rectangular FGPS plate deflection

increases as the PVI increases.

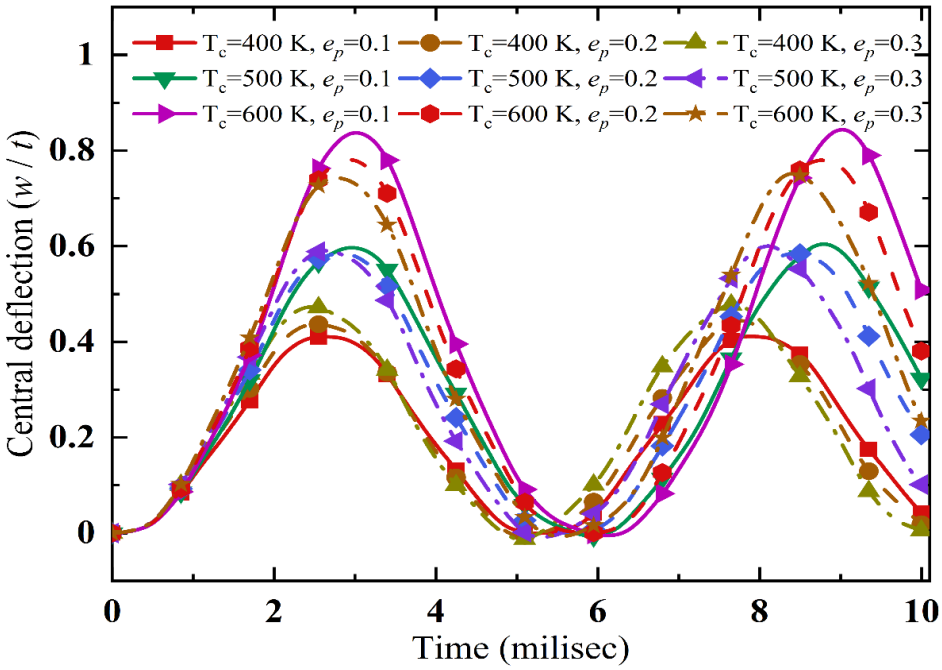

Figure 5. Influence of PVI on central deflections ($\breve{w}_c = w/t$) for temperature rise. (*a/b* = 1, *a/t* = 30, *m* = 2, *Φ* =0°, SSSS, and $P_d = P_e$).

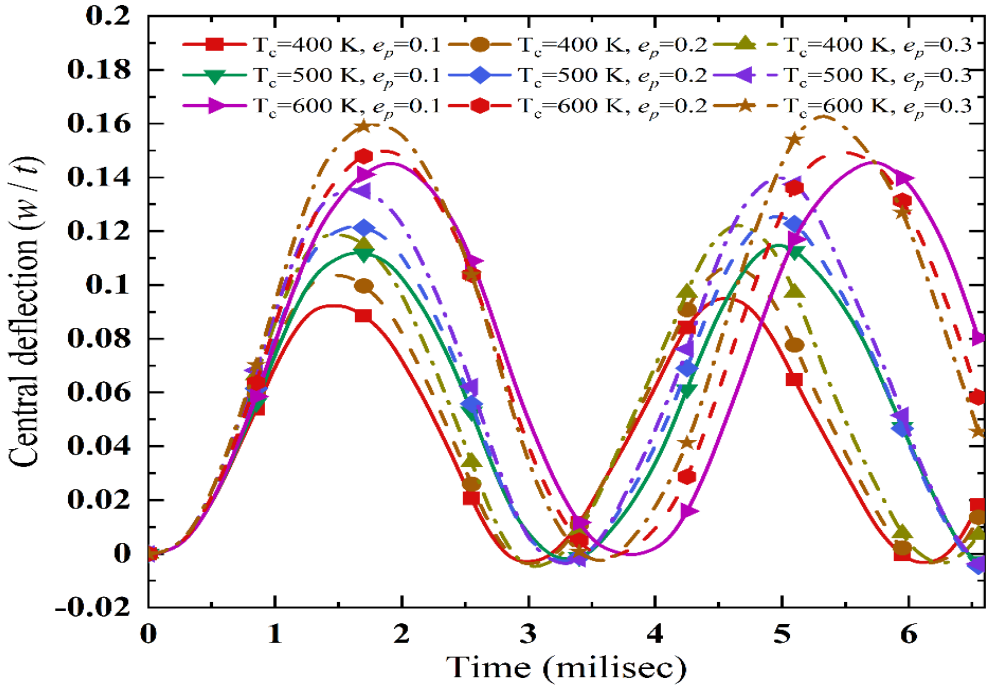

Figure 6. Influence of PVI on central deflections ($\breve{w}_c = w/t$) for temperature rise. (*a/b* = 1, *a/t* = 30, *m* = 2, *Φ* =40°, SSSS, and $P_d = P_e$).

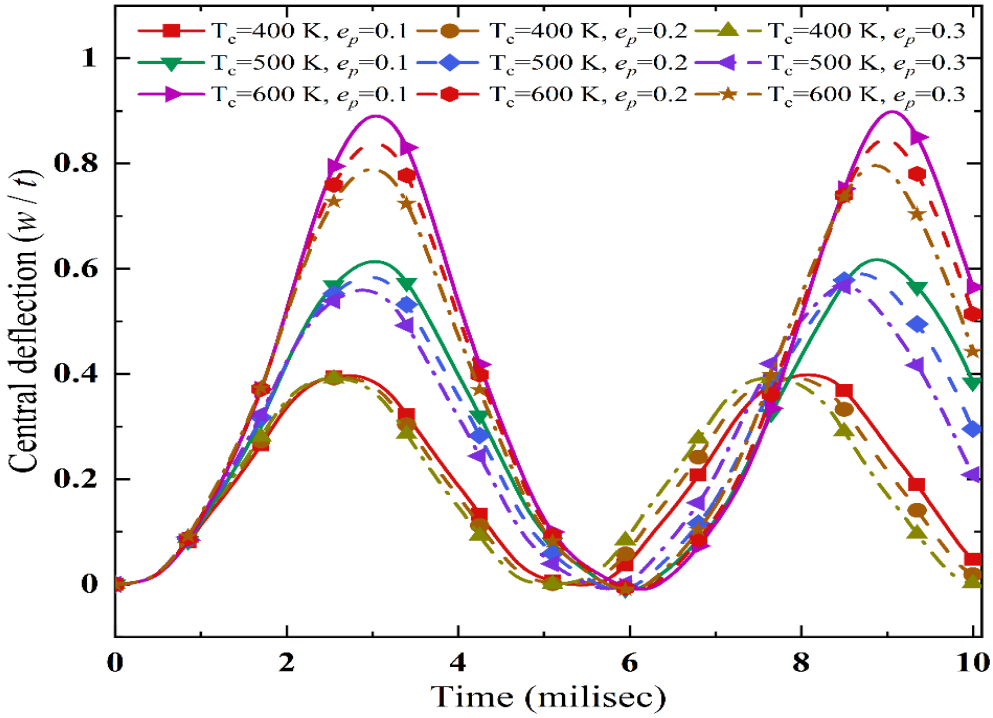

Figure 7. Influence of PVI on central deflections ($\breve{w}_c = w/t$) for temperature rise. (*a/b* = 1, *a/t* = 30, *m* = 2, *Φ* =0°, SSSS, and $P_d = P_c$).

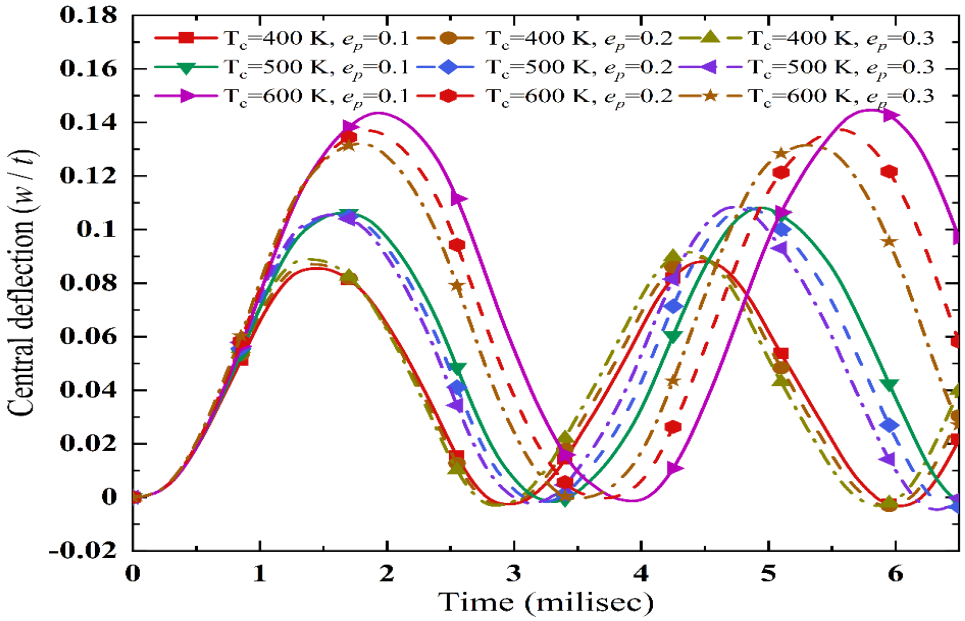

Figure 8. Influence of PVI on central deflections ($\breve{w}_c = w/t$) for temperature rise. (*a/b* = 1, *a/t* = 30, *m* = 2, *Φ* =40°, SSSS, and $P_d = P_c$).

In contrast, the deflection decreases for higher temperatures as the PVI increases (T_c = 600 K). Furthermore, for any given temperature of the angled plate and EDP distribution, the deflection increases as the PVI increases. In comparison, the trend is reversed for CDP distribution. This is due to the porous effect that causes the plate stiffness to decrease. For porosity distributions of type P_c, it could be because more material accretion away from the

middle surface leads to the FGPS plate's high flexural stiffness. Meanwhile, the porosity dispersion in the Pe results in consistent material distribution over the thickness, decreasing stiffness. The impact of thermal loading on the geometrically nonlinear transient response of the FGPS plate reveals that as the temperature rises, the amplitude and time period of motion increase. Moreover, Figures. 5 – 8 show that under thermal loadings, for the square porous FG plates, the Pc has the highest transient deflections ($P_c > P_e$), and the pattern is reversed for skewed FGPS plates ($P_e > P_c$). It may be due to the distribution of the porosities leading to the stiffness variation. In addition, the FGPS plate with Pc has higher stiffness for a given skew angle than the Pe due to the distribution of porosities.

7.2. Effect of Volume fraction grading index

Figures 9 – 12 demonstrate the impact of the VFGI for P_e and P_c type porosity distributions on the geometrically nonlinear transient response of the FGPS plate in a thermal environment. It can be seen that with an increase in the VFGI (m) and temperature, the amplitude and time-period of motion increase. Therefore, the magnitude of deflection is reduced when bending rigidity increases. The metallic plate has the highest vibration amplitude, whereas the ceramic plate has the lowest. This is due to a decline in the ceramic composition of the plate as m rises. As a result, the FGPS plate's stiffness decreases as the VFGI rises but increases as the skew angle rise. Thus, increasing the skew angle reduces the plate's transient deflection. Therefore, the influence of VFGI seems to be predominant for property determination of the FGPS plate, which is subsequently proportional to the stiffness. Figs. 9 – 12 show that for each value of m and temperature, the P_e type of distribution has the lowest geometrically nonlinear transient deflections. On the other hand, the P_c type has the highest ($P_c > P_e$). As a result, the porosity distribution affects the FGPS plate's deflection. It may be because the distribution of materials in the plate depends on the arrangement of porosities and temperature, which leads to the variation of stiffness.

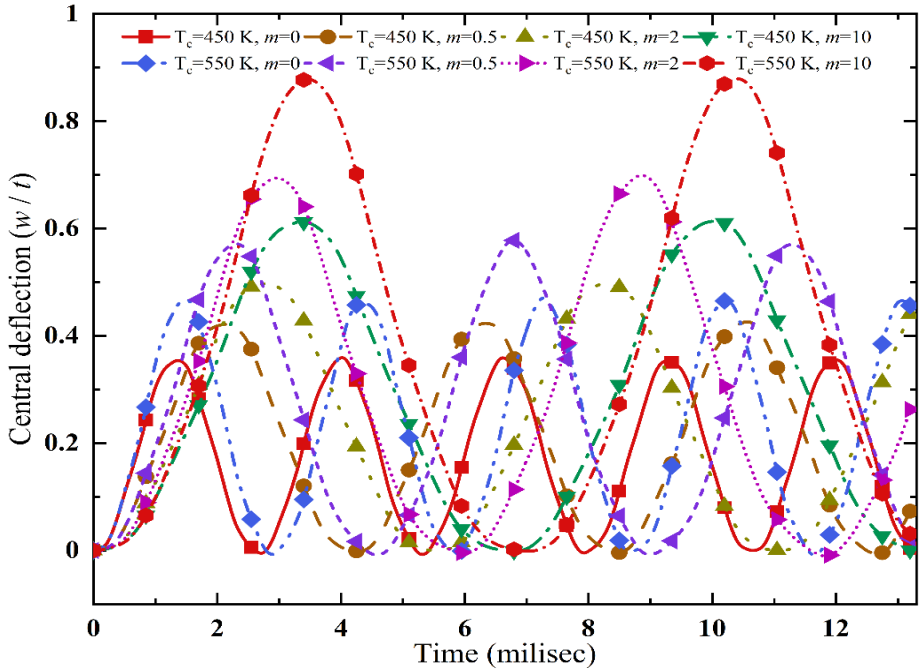

Figure 9. Influence of VFGI (*m*) on the central deflections ($\breve{w}_c = w/t$) for temperature rise. (*a/b* = 1, *a/t* = 30, e_p = 0.15, Φ =0°, SSSS, and $P_d = P_e$).

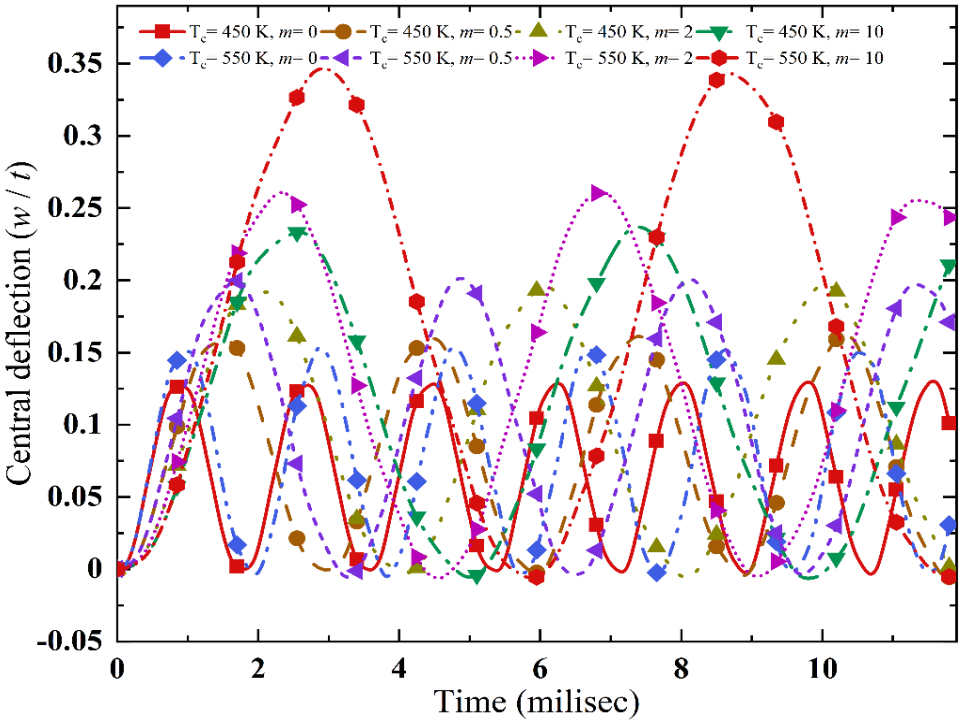

Figure 10. Influence of VFGI (*m*) on central deflections ($\breve{w}_c = w/t$) for temperature rise. (*a/b* = 1, *a/t* = 30, e_p = 0.15, Φ =30°, SSSS, and $P_d = P_e$).

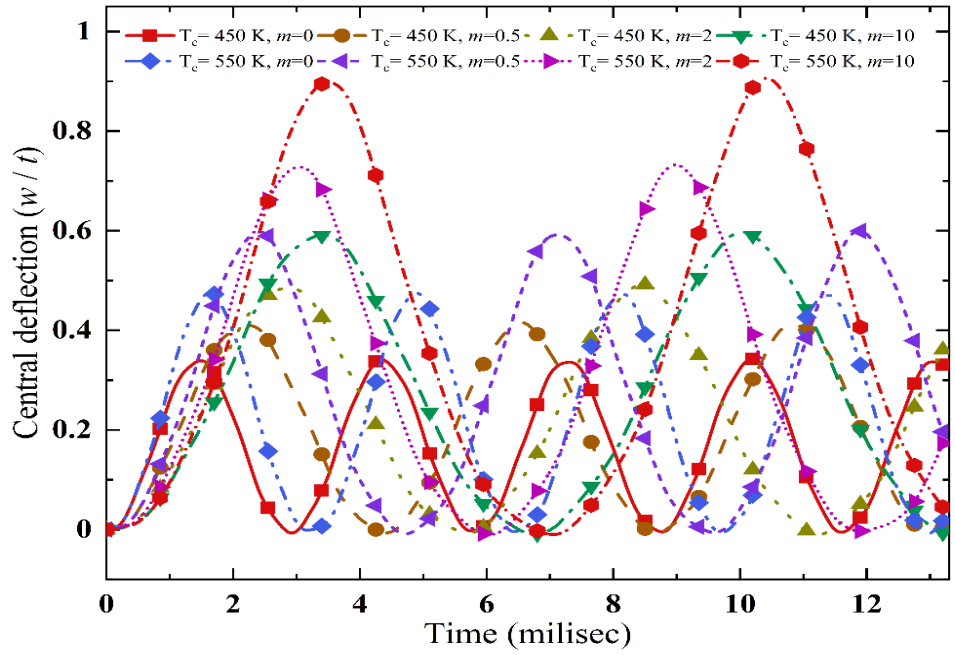

Figure 11. Influence of VFGI (m) on central deflections ($\breve{w}_c = w/t$) for temperature rise. (*a/b* = 1, *a/t* = 30, e_p = 0.15, Φ =0°, SSSS, and $P_d = P_c$).

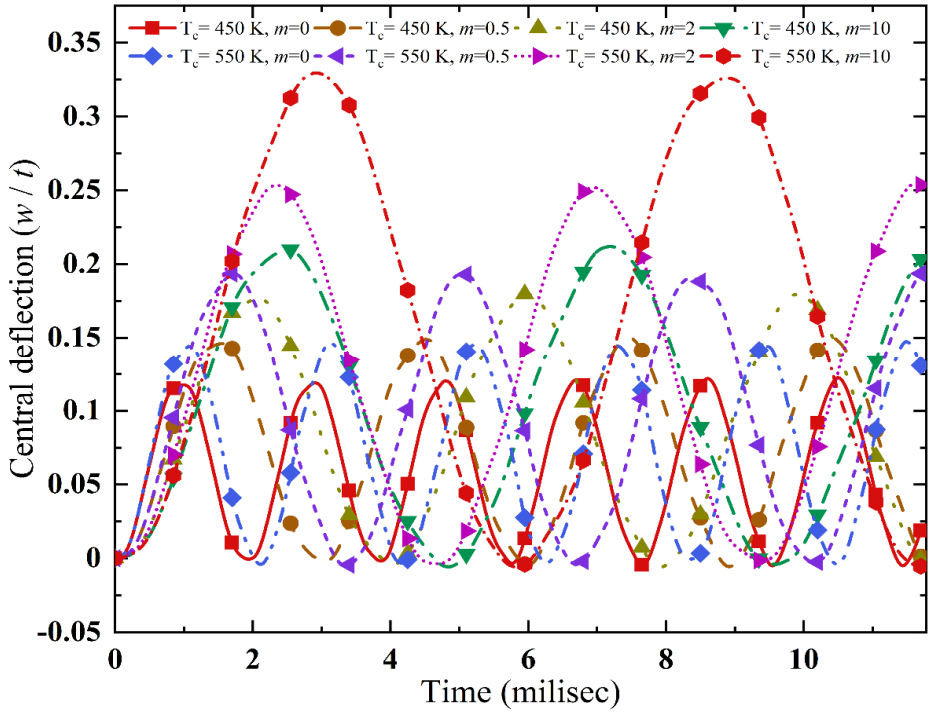

Figure 12. Influence of VFGI (*m*) on central deflections ($\bar{w}_c = w/t$) for temperature rise. (*a*/*b* = 1, *a*/*t* = 30, e_p = 0.15, Φ =30°, SSSS, and $P_d = P_c$).

8. Conclusions

This article investigates the effects of porosity distributions on geometrically nonlinear transient deflections of geometrically skewed functionally graded plates with porosity in a thermal environment. By combining the FSD theory with von Kármán assumptions, nonlinear FE formulations were generated. The temperature-dependent effectual material properties are estimated using a modified power-law series, which accounts for the different porosity distributions. The following observations are made from the detailed parametric evaluation. As the volume fraction grading index and temperature rise, the FGPS plate's geometrically nonlinear transient deflection increases in a thermal environment. However, as the skew angle increases, the deflection decreases. The EDP (P_e) distribution exhibits a minor influence, whereas the CDP (P_c) distribution substantially impacts geometrically nonlinear deflections. The impact of an increase in the Porosity Volume Index on deflection is more pronounced at higher temperatures for a skewed plate in the case of CDP, compared to EDP.

Declaration of competing interest:

None.

REFERENCES:

[1] Wattanasakulpong N, Gangadhara Prusty B, Kelly DW, Hoffman M. Free vibration analysis of layered functionally graded beams with experimental validation. Mater Des 2012;36:182–90. https://doi.org/10.1016/j.matdes.2011.10.049.

[2] Wang YQ, Yang Z. Nonlinear vibrations of moving functionally graded plates containing porosities and contacting with liquid: internal resonance. Nonlinear Dyn 2017;90:1461–80. https://doi.org/10.1007/s11071-017-3739-z.

[3] Cong PH, Chien TM, Khoa ND, Duc ND. Nonlinear thermomechanical buckling and post-buckling response of porous FGM plates using Reddy's HSDT. Aerosp Sci Technol 2018;77:419–28. https://doi.org/10.1016/j.ast.2018.03.020.

[4] Nam VH, Phuong NT, Dong DT, Trung NT, Tue N Van. Nonlinear thermo-mechanical buckling of higher-order shear deformable porous functionally graded material plates reinforced by orthogonal and/or oblique stiffeners. Proc Inst Mech Eng Part C J Mech Eng Sci 2019;233:6177–96. https://doi.org/10.1177/0954406219861658.

[5] Huang X-L, Dong L, Wei G-Z, Zhong D-Y. Nonlinear free and forced vibrations of porous sigmoid functionally graded plates on nonlinear elastic foundations. Compos Struct 2019;228:111326. https://doi.org/10.1016/j.compstruct.2019.111326.

[6] Phung-Van P, Thai CH, Ferreira AJM, Rabczuk T. Isogeometric nonlinear transient analysis of porous FGM plates subjected to hygro-thermo-mechanical loads. Thin-Walled Struct 2020;148:106497. https://doi.org/10.1016/j.tws.2019.106497.

[7] Xie K, Wang Y, Niu H, Chen H. Large-amplitude nonlinear free vibrations of functionally graded plates with porous imperfection: A novel approach based on energy balance method. Compos Struct 2020;246:112367. https://doi.org/10.1016/j.compstruct.2020.112367.

[8] Saleh B, Jiang J, Fathi R, Al-hababi T, Xu Q, Wang L, et al. 30 Years of functionally graded materials: An overview of manufacturing methods, Applications and Future Challenges. Compos Part B Eng 2020;201:108376. https://doi.org/10.1016/j.compositesb.2020.108376.

[9] Sundararajan N, Prakash T, Ganapathi M. Nonlinear free flexural vibrations of functionally graded rectangular and skew plates under thermal environments. Finite Elem Anal Des 2005;42:152–68. https://doi.org/10.1016/j.finel.2005.06.001.

[10] Taj MG, Chakrabarti A, Talha M. Bending analysis of functionally graded skew sandwich plates with through-the thickness displacement variations. J Sandw Struct Mater 2014;16:210–48. https://doi.org/10.1177/1099636213512499.

[11] Parida S, Mohanty SC. Thermoelastic vibration analysis of functionally graded skew plate using nonlinear finite element method. J Therm Stress 2017;40:1111–33. https://doi.org/10.1080/01495739.2017.1290513.

[12] Tomar SS, Talha M. On the flexural and vibration behavior of imperfection sensitive higher order functionally graded material skew sandwich plates in thermal environment. Proc Inst Mech Eng Part C J Mech Eng Sci 2019;233:1271–88. https://doi.org/10.1177/0954406218766959.

[13] Kumar H S N, Kattimani S, Nguyen-Thoi T. Influence of porosity distribution on nonlinear free vibration and transient responses of porous functionally graded skew plates. Def Technol 2021;17:1918–35. https://doi.org/10.1016/j.dt.2021.02.003.

[14] Huang X-L, Shen H-S. Nonlinear vibration and dynamic response of functionally graded plates in thermal environments. Int J Solids Struct 2004;41:2403–27. https://doi.org/10.1016/j.ijsolstr.2003.11.012.

[15] Javaheri R, Eslami MR. Thermal buckling of functionally graded plates based on higher order theory. J Therm Stress 2002;25:603–25. https://doi.org/10.1080/01495730290074333.

[16] Javaheri R, Eslami MR. Thermal Buckling of Functionally Graded Plates. AIAA J 2002;40:162–9. https://doi.org/10.2514/2.1626.

[17] Praveen GN, Reddy JN. Nonlinear transient thermoelastic analysis of functionally graded ceramic-metal plates. Int J Solids Struct 1998;35:4457–76. https://doi.org/10.1016/S0020-7683(97)00253-9.

[18] Naveen Kumar HS, Kattimani S. Effect of different geometrical non-uniformities on nonlinear vibration of porous functionally graded skew plates: A finite element study. Def Technol 2022;18:918–36. https://doi.org/10.1016/j.dt.2021.05.002.

[19] Hosur Shivaramaiah NK, Kattimani S, Shariati M, Nguyen-Thoi T. Geometrically nonlinear behavior of two-directional functionally graded porous plates with four different materials. Proc Inst Mech Eng Part C J Mech Eng Sci 2022;236:11008–23. https://doi.org/10.1177/09544062221111038.

[20] Naveen Kumar HS, Kattimani S, Marques FD, Nguyen-Thoi T, Shariati M. Geometrically Nonlinear Study of Functionally Graded Saturated Porous Plates Based on Refined Shear Deformation Plate Theory and Biot's Theory. Int J Struct Stab Dyn 2023;23. https://doi.org/10.1142/S021945542350013X.

[21] Kattimani SC, Ray MC. Control of geometrically nonlinear vibrations of functionally graded magneto-electro-elastic plates. Int J Mech Sci 2015;99:154–67. https://doi.org/10.1016/j.ijmecsci.2015.05.012.

[22] Kumar HSN, Kattimani S. Nonlinear analysis of two - directional functionally graded doubly curved panels with porosities. Struct Eng Mech 2022;82:477–90. https://doi.org/10.12989/sem.2022.82.4.477.

[23] Finney RH. Application of Finite Element Analysis. vol. 119. 4th Editio. JohnWiley & Sons (Asia) Pvt. Ltd.,; 1987.

[24] Kiran MC, Kattimani SC, Vinyas M. Porosity influence on structural behaviour of skew functionally graded magneto-electro-elastic plate. Compos Struct 2018;191:36–77. https://doi.org/10.1016/j.compstruct.2018.02.023.

[25] Han W, Petyt M. Geometrically nonlinear vibration analysis of thin, rectangular plates using the hierarchical finite element method—I: The fundamental mode of isotropic plates. Comput Struct 1997;63:295–308. https://doi.org/10.1016/S0045-7949(96)00345-8.

[26] Reddy JN, Chin CD. Thermomechanical analysis of functionally graded cylinders and plates. J Therm Stress 1998;21:593–626. https://doi.org/10.1080/01495739808956165.

[27] Liew KM, Xiang Y, Kitipornchai S, Wang CM. Vibration Of Thick Skew Plates Based On Mindlin Shear Deformation Plate Theory. J Sound Vib 1993;168:39–69. https://doi.org/10.1006/jsvi.1993.1361.

[28] Rezaei AS, Saidi AR, Abrishamdari M, Mohammadi MHP. Natural frequencies of functionally graded plates with porosities via a simple four variable plate theory: An analytical approach. Thin-Walled Struct 2017;120:366–77. https://doi.org/10.1016/j.tws.2017.08.003.

[29] Chen J, Dawe D. J, Wang S. Nonlinear transient analysis of rectangular composite laminated plates. Compos Struct 2000;49:129–39. https://doi.org/10.1016/S0263-8223(99)00108-7.